Thin-thick surface phase coexistence and boundary tension of the square-well fluid on a weak attractive surface

Jayant K. Singh, Gautam Sarma, and Sang K. Kwak

Citation: The Journal of Chemical Physics **128**, 044708 (2008); doi: 10.1063/1.2824503

View online: http://dx.doi.org/10.1063/1.2824503

View Table of Contents: http://scitation.aip.org/content/aip/journal/jcp/128/4?ver=pdfcov

Published by the AIP Publishing

Thin-thick surface phase coexistence and boundary tension of the square-well fluid on a weak attractive surface

Jayant K. Singh[a] and Gautam Sarma
Department of Chemical Engineering, Indian Institute of Technology, Kanpur 208016, India

Sang K. Kwak
Division of Chemical and Biomolecular Engineering, School of Chemical and Biomedical Engineering, Nanyang Technological University, Singapore 637459, Singapore

(Received 27 August 2007; accepted 21 November 2007; published online 28 January 2008)

Prewetting transition is studied for the square-well fluid of attractive-well diameter $\lambda_{ff}\sigma_{ff}=1.5$ in the presence of a homogeneous surface modeled by the square-well potential of attractive well from $0.8\sigma_{ff}$ to $1.8\sigma_{ff}$. We investigate surface phase coexistence of thin-thick film transition using grand-canonical transition matrix Monte Carlo (GC-TMMC) and histogram reweighting techniques. Molecular dynamics (MD) and GC-TMMC are utilized to predict the properties of the fluid for various surface fluid affinities. Occurrences of prewetting transition with the variation of surface affinity are observed for a domain of reduced temperature from $T^*=0.62$ to 0.75. We have used MD and GC-TMMC+finite size scaling (FSS) simulations to calculate the boundary tension as a function of temperature as well as surface affinity. Boundary tensions via MD and GC-TMMC +FSS methods are in good agreement. The boundary tension increases with the decrease of wall-fluid affinity. Prewetting critical properties are calculated using rectilinear diameter approach and scaling analysis. We found that critical temperature and density increase with the decrease of wall-fluid affinity. © *2008 American Institute of Physics*. [DOI: 10.1063/1.2824503]

I. INTRODUCTION

Morphological transition in the presence of surfaces plays an important role in various industrial applications. Relative strengths of surface-fluid and fluid-fluid interactions can lead to various phase transitions such as prewetting, layering, and capillary condensation.[1] Coexistence phases of vapor and liquid in contact with an attractive solid surface can induce two different kinds of phenomena. For strong attractive surface the fluid molecules spread across the surface (in the form of thick film), leading to complete *wetting* of the surface. On the other hand, a nonwetting behavior is exhibited, if the fluid molecules are weakly adsorbed on the surface, so that the interactions between the fluid molecules becomes stronger than those between the wall and the fluid molecules.[2] In such case partial wetting occurs in the adsorbed film, which consists of a layer of vapor bubbles and liquid drops. Wetting transition is closely associated with a temperature called wetting temperature T_w at which adsorption state transforms from partial wetting to complete wetting. Below the wetting temperature the thickness of the film adsorbed on the surface remains finite at all pressures, which are below the bulk saturation pressure. Above wetting temperature, prewetting transition occurs when there is a first order transition between the thin and thick films adsorbed on the surface. This prewetting transition terminates at prewetting critical point T_{cpw}, where thin and thick films (surface states) become indistinguishable. In 1977, Cahn[2] predicted the existence of wetting transition through a two-phase mixture of fluids near a third phase, surface. Independently, Ebnar and Saam[3] also predicted wetting and prewetting transition of argon film adsorbed onto a weakly attractive solid carbon dioxide surface. The authors used the density functional theory (DFT) for the prediction of wetting transition. Since then, DFT has been widely used to study wetting phenomena.[4] Experimental evidences, which came much later, support the prediction of prewetting transitions. Examples can be found for helium adsorption on Cs (Refs. 5 and 6) and Rb,[7] liquid hydrogen on various substrates,[8] and acetone on graphite.[9]

Phase transition in the presence of surfaces has been studied using various molecular simulation techniques in addition to theory and experiments. Finn and Monson[10] were first to study the prewetting transition of argon molecules on solid carbon dioxide system using isothermal-isobaric Monte Carlo (MC) method. Subsequently, few more groups have utilized different molecular simulation methodologies[11–14] to understand the prewetting transition. Phase equilibria calculations of the thin-thick film have become much easier with the advent of simulation techniques such as transitional matrix Monte Carlo (TMMC),[15] multicanonical sampling,[16] and histogram reweighting.[17] Errington recently revisited the prewetting transitions of model argon on solid carbon dioxide and successfully demonstrated the use of grand-canonical transitional matrix Monte Carlo (GC-TMMC) to predict the wetting temperature[18] and boundary tension.[19] In this work, we investigate prewetting transitions of a model system based on square-well potential and demonstrate the equivalence of MC and molecular dynamics (MD) methods in the calculation of boundary tension. Also, GC-TMMC method is

[a]Author to whom correspondence should be addressed. Electronic mail: jayantks@iitk.ac.in.

used to study the first order wetting behavior of a square-well fluid in the extreme range of potential parameters. In prediction of boundary tension of the thin-thick film, the concept of finite size scaling (FSS) method has attracted less attention and hence forms a secondary object of our study. We utilize MD and GC-TMMC simulations to explore the thermodynamics of thin-thick film phases on a surface and present comparison of the results via the above two methods. The paper is organized as follows. Section II describes the models used in this study as well as our simulation methods. Section III presents the results of phase coexistence of thin-thick films with the variation of the strength of substrate potential and the details of boundary tension calculation using MD as well as GC-TMMC simulations. Section IV concludes our study.

II. MODEL AND METHODOLOGY

One of the simple pair potentials containing both the attractive and repulsive forces is square-well (SW) potential. Owing to its simplicity, this model has been widely used to study phenomena related to phase coexistence and interfacial properties of simple fluid.[20–27] Henderson and Swol[28] used SW model to understand wetting transition. The SW potential is also used as a model for the colloidal[29–31] and globular protein solutions.[32,33] In this work fluid-fluid interaction is modeled as SW potential, which is represented as

$$U_{ff}(r) = \infty \quad \text{if } r < \sigma_{ff}$$
$$= -\varepsilon_{ff} \quad \text{if } \sigma_{ff} \leqslant r < \lambda_{ff}\sigma_{ff}$$
$$= 0 \quad \text{if } r \geqslant \lambda_{ff}\sigma_{ff} \tag{1}$$

where σ_{ff}, ε_{ff}, and λ_{ff} are hard sphere diameter, potential well depth, and well diameter of fluid-fluid potential, respectively. Fluid-wall interaction is also modeled by the following SW-type potential:

$$U_{wf}(z) = \infty \quad \text{if } z < 0.8\sigma_{ff}$$
$$= -\varepsilon_{wf} \quad \text{if } 0.8\sigma_{ff} \leqslant z < \lambda_{wf}\sigma_{ff}$$
$$= 0 \quad \text{if } z \geqslant \lambda_{wf}\sigma_{ff}, \tag{2}$$

where ε_{wf} and λ_{wf} are corresponding parameters for fluid-substrate potential. In this work, units are adopted such that σ_{ff} and ε_{ff} are unity and $\lambda_{ff}=1.5$ and $\lambda_{wf}=1.8$. Wall-fluid interaction ε_{wf} is varied from 2 to 5 in units of ε_{ff}. All lengths are in units of core diameter σ_{ff}.

In grand-canonical ensemble, for a fixed temperature T, chemical potential μ, and volume V, the probability of visiting a microstate s with particles $N(s)$ and configuration energy $E(s)$ probability is given by the following expression:

$$\pi(s) = \frac{1}{\Xi}\left[\frac{V^{N(s)}}{\Lambda^{3N(s)}N(s)!}\right]\exp[-\beta E(s)]\exp[\beta\mu N(s)], \tag{3}$$

where Ξ is grand-canonical partition function, Λ is de Broglie wavelength, $\beta=1/k_BT$, and k_B is Boltzmann's constant.

We adopted the methodology as shown in Ref. 18 to get the macrostate probability from the probability transition matrix. We employed the possible state changes by deletion, addition, and displacement of MC moves. For the moves $S \to S$, $S \to S-1$, and $S \to S+1$, the detailed balance can be simplified to give the macrostate probability as

$$\ln \Pi(S+1) = \ln \Pi(s) - \ln\left[\frac{P(S+1 \to S)}{P(S \to S+1)}\right]. \tag{4}$$

To enhance the probability of transition from one phase to another phase, we utilize multicanonical sampling[16] with a weighting function $\eta(S)=-\ln \Pi(S)$. We modify the acceptance criteria in the presence of the bias as follows:

$$a(s \to t) = \min\left[1, \frac{\exp[\eta(T)]\pi(t)}{\exp[\eta(S)]\pi(s)}\right]. \tag{5}$$

Histogram reweighting techniques[17] is used to obtain the chemical potential that gives the phase coexistence of the thin-thick film.

We use Binder formalism[34] to calculate infinite size boundary tension, between thin and thick films, from a series of finite size calculations. If τ_L is interfacial tension for a system of box length L, then the τ boundary tension for infinite system is given by

$$\beta\tau_L = \frac{\beta F_L}{2L} = C_1\frac{1}{L} + C_2\frac{\ln(L)}{L} + \beta\tau, \tag{6}$$

where c_1 and c_2 are constants and F_L represents the free energy of the thin-thick interface for a finite system size L.

Helmholtz potential, for the thin-thick film on a substrate (see Fig. 1), for the infinitesimal and reversible transformation is given by

$$dF = -PHdA - PAdH - SdT + \mu dN + \tau dL_y, \tag{7}$$

where F is the Helmholtz free energy, A is the substrate area, H is the distance between the upper wall and the substrate, S is the entropy, τ is the boundary tension between thin and thick films on the substrate, P is the pressure, and T is the temperature. Expression above has taken into account implicitly that the change in the density is across the x direction.

For a constant substrate area A, H, the total number of particles N, and T, the boundary tension is expressed as follows:

$$\tau = \left(\frac{\partial F}{\partial L_y}\right)_{A,H,N,T}. \tag{8}$$

Above equation can be related to pressure components by simple mathematical manipulation,

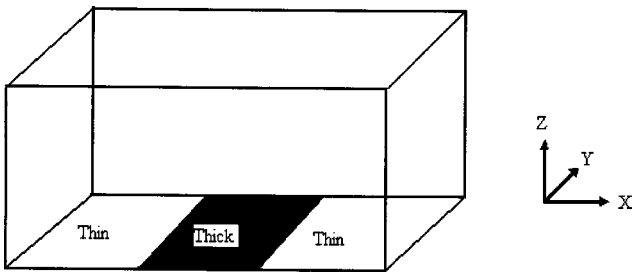

FIG. 1. Schematic representation of the thin-thick film over a solid surface.

$$\left(\frac{\partial F}{\partial L_y}\right)_{A,H,N,T} = HL_x\left[\left(\frac{\partial F}{\partial V}\right)_{L_x,H,N,T} - \left(\frac{\partial F}{\partial V}\right)_{L_y,H,N,T}\right]$$
$$= HL_x[P_{xx} - P_{yy}]. \quad (9)$$

Hence, thin-thick boundary tension is given by

$$\tau = \frac{HL_x[P_{xx} - P_{yy}]}{2}. \quad (10)$$

The factor "2" in Eq. (10) accounts for the two interfaces in the simulations. P_{xx} is the pressure tensor component in the x direction, which is perpendicular to the thin-thick film interface (see Fig. 1). P_{yy} is the pressure tensor component in the y direction, which is parallel to the thin-thick film interface.

Pressure-tensor components, in this work, are obtained from the virial formalism.[35] For pairwise-additive potentials the expression is

$$p_{\alpha\beta} = \rho k_B T + \frac{1}{V}\left\langle \sum_{i=1}^{N-1} \sum_{j>i}^{N} (\mathbf{r}_{ij})_\alpha (\mathbf{f}_{ij})_\beta \right\rangle, \quad (11)$$

where ρ is the number density, $\mathbf{r}_{ij}$ is the vector between the center of mass of molecules i and j, and $\mathbf{f}_{ij} = -\nabla u_{ij}$ is the force between them; the angle brackets indicate ensemble or time average. For discontinuous potential such as those used in this study, the forces are impulsive, having infinite magnitude but acting for an infinitesimal time. When integrated over time each collision contributes a well-defined amount to the average in the following expression:

$$p_{\alpha\beta} = \rho k_B T + \frac{1}{V t_{\text{sim}}} \sum_{\text{collisions}} (\mathbf{r}_{ij})_\alpha (\Delta \mathbf{p}_{ij})_\beta, \quad (12)$$

where t_{sim} is the total simulation time and the sum is over all collisions occurring in this time; $\Delta \mathbf{p}_{ij}$ is the impulse associated with the collision between molecules i and j.

Prewetting critical temperature has been calculated in the literature using various techniques.[11,36] In this work, we have estimated the critical parameters of the thin-thick film by using the coexistence data and the least squares fit of the following scaling law:

$$(N/A)_l - (N/A)_v = C\left(1 - \frac{T}{T_{\text{cpw}}}\right)^{\beta_c}, \quad (13)$$

where $(N/A)_l$ and $(N/A)_v$ are surface densities of thick and thin films, respectively, and C and β_{cpw} are fitting parameters. The critical temperature T_{cpw} estimated from Eq. (13) is used to calculate the critical density $(N/A)_c$ from the least squares fit of the following equation:

$$\frac{(N/A)_l + (N/A)_v}{2} = (N/A)_c + D(T - T_c), \quad (14)$$

where D is a fitting parameter.

One side of the simulation box was chosen as a surface plane with attractive square-well potential. The opposite side was chosen to be repulsive wall to keep the fluid inside the simulation box. The height of the box was set to a fixed value of 20 in z direction (see Fig. 1) to avoid the effect of repulsive wall on the attractive surface. The other sides of the box L_x and L_y were equal in length in GC-TMMC simulations. The lateral variation of the box in these two dimensions represents varied system sizes with surface areas of $L_x \times L_y$. GC-TMMC simulations for calculating surface thin-thick saturated densities and pressures are conducted on AMD Opteron CPUs. Although simulations can be done using single CPU, we utilized the parallizable nature of transition matrix and used 8–20 CPUs to calculate the data. Four independent runs were performed to calculate the statistical error.

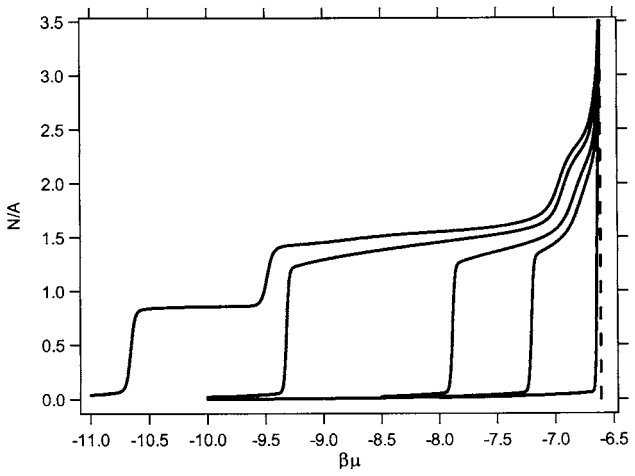

FIG. 2. Adsorption isotherm plot of surface density vs chemical potential at $T^* = 0.68$. Lines from left to right correspond to the wall-fluid interaction strengths, $\varepsilon_{wf} = 4.0$, 3.0, 2.5, and 2.0, respectively. The dotted line represents the bulk coexistence chemical potential.

MD has been previously used to determine the prewetting transition.[14] In current investigation, we have utilized the method for the calculation of boundary tension and compared the performance with that of GC-TMMC. Initially, we place molecules on the attractive surface of the simulation box with L_z constant (same as in GC-TMMC) such that initial surface density is slightly higher than coexistence surface density of the thick film. Second step is to create a vacuum by expanding the simulation cell in x direction such that $L_x = 3L_y$. Periodic boundary condition is applied only in x and y directions. MD simulations are conducted using ETOMICA[37] package. Equilibration period is performed in a canonical (NVT) ensemble. During equilibration, the temperature was kept constant by momentum scaling, with all momenta multiplied by an appropriate factor at the end of each time step such that the total kinetic energy of the system is consistent with the equipartition value of the temperature.[35] Production period is conducted in microcanonical (NVE) ensemble. The reduced time step Δt^* (in units of $\sigma\sqrt{m/\varepsilon}$) was fixed at 0.04. The simulations were conducted with the system size of 2000 particles. We have taken 10^5 time steps as equilibration period and equal number for production steps.

III. RESULTS AND DISCUSSIONS

We first present the adsorption isotherms calculated using GC-TMMC simulation and histogram reweighting technique. The isotherms were calculated for a system corresponding to simulation box size of $9 \times 9 \times 20$ for which maximum number of particles in the GCMC simulations was kept at 300. Figure 2 presents the surface density (number of

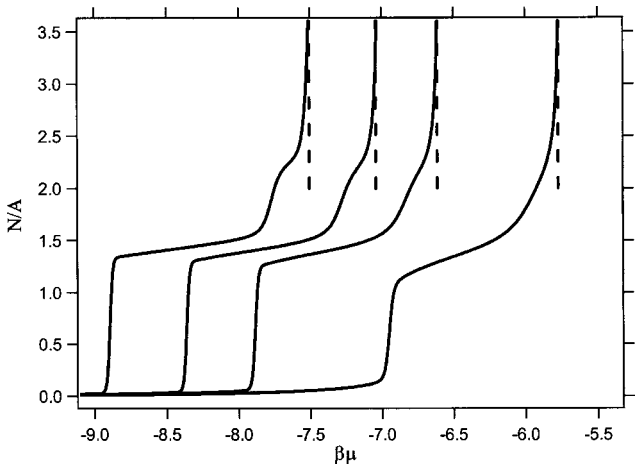

FIG. 3. Plot of adsorption isotherms of surface density vs chemical potential for wall-fluid interaction potential, ε_{wf}=3.0. The isotherms from left to right are for T^*=0.62, 0.65, 0.68, and 0.75, respectively. Dotted lines represent the corresponding bulk coexistence chemical potential for different temperatures.

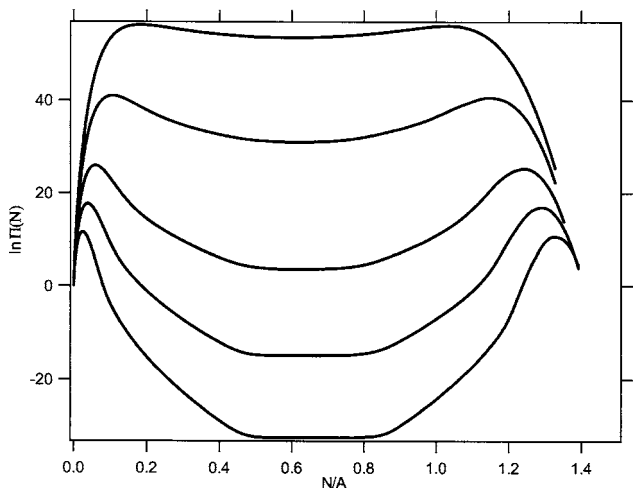

FIG. 4. Coexistence surface density probability distribution of thin-thick film for ε_{wf}=3.0. The lines from the bottom are for the temperatures T^* =0.62, 0.65, 0.68, 0.7, and 0.72.

molecules per unit surface area) as a function of chemical potential for various wall-fluid affinity at a constant temperature $T^*=kT/\varepsilon_{ff}$=0.68. At a very low chemical potential a thin vapor film is deposited on the surface. As we increase the chemical potential, we observe a jump in the surface density. This jump occurs at a certain value of chemical potential lesser than that for the bulk vapor-liquid coexistence phase (shown as dashed line). Further increase in the chemical potential toward bulk vapor-liquid chemical potential leads to a state, where liquid is spread on the surface. Similar behavior is observed for different wall-fluid affinities, viz., ε_{wf}=2.5–4.0. This discontinuous change in the density represents the prewetting transition and implicitly indicates the value of the prewetting chemical potential. From Fig. 2, it is evident that the prewetting chemical potential increases with the decrease in the wall-fluid affinity. For weaker attractive surface, ε_{wf}=2.0, prewetting transition disappears. For relatively stronger attractive surface than ε_{wf}=4.0, layering behavior in the adsorption isotherms is observed, as shown for ε_{wf}=5.0 in the Fig. 2. Number of layers increase with the increase in the wall-fluid interaction (not shown in the figure). Prewetting transition is also found to be sensitive with respect to the temperature of the system. Figure 3 shows the adsorption isotherms for ε_{wf}=3.0 for different temperatures. As the temperature increases, the density of thick film decreases and that of thin film increases. Prewetting chemical potential increases with the increase of temperature.

Figure 4 shows the thin-thick coexistence surface density probability distribution for ε_{wf}=3.0 for different temperatures. Such distribution is evaluated at prewetting chemical potential. To determine prewetting chemical potential from the probability distribution generated at chemical potential away from the coexistence chemical potential, the distribution data are reweighted until areas under two peaks, corresponding to thin- and thick-film phases, are equal.

Figure 5 presents the results of surface phase coexistence of the thin-thick film as a function of temperature for different wall-fluid interaction energies ε_{wf} using GC-TMMC. These calculations were made using simulation box size of $9\times9\times20$. Maximum number of molecules for the simulation was kept at 300. Effect of wall-fluid interaction seems insensitive on the thin-film density at lower temperature. However, as the temperature increases, the thin-film density is distinctly increased for higher ε_{wf}. Contrary to the thin-film case, the effect of wall-fluid interaction is prominent on the thick-film density. There are distinguishable differences in the densities of thick films even at lower temperature. Simulation data presented in Fig. 5 indicate that at a given temperature surface density of thick film is found to be higher for the case of weak attractive surface. To understand the effect of wall-fluid affinity on the structure of thin and thick films, MD simulations are conducted for various wall-fluid interaction strengths. Figure 6 presents the density profiles of thin-thick film phases for T^*=0.68. Two peaks are observed in both phases for different wall-fluid affinities. The peaks are observed at L_z=0.8 and 1.8, respectively. Density for the two layers formed for the surface film is higher for

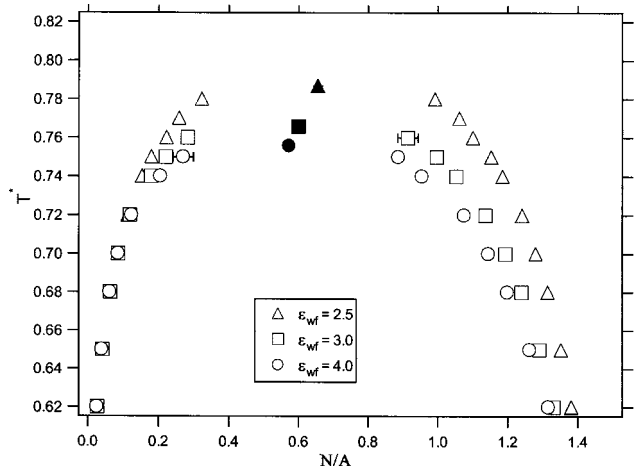

FIG. 5. Temperature against surface density plot of thin-thick film of SW fluid for wall-fluid interaction strengths, ε_{wf}=2.5, 3.0, and 4.0. Open symbols represent data calculated from GC-TMMC+histogram reweighting analysis. Filled symbols correspond to the estimated critical points.

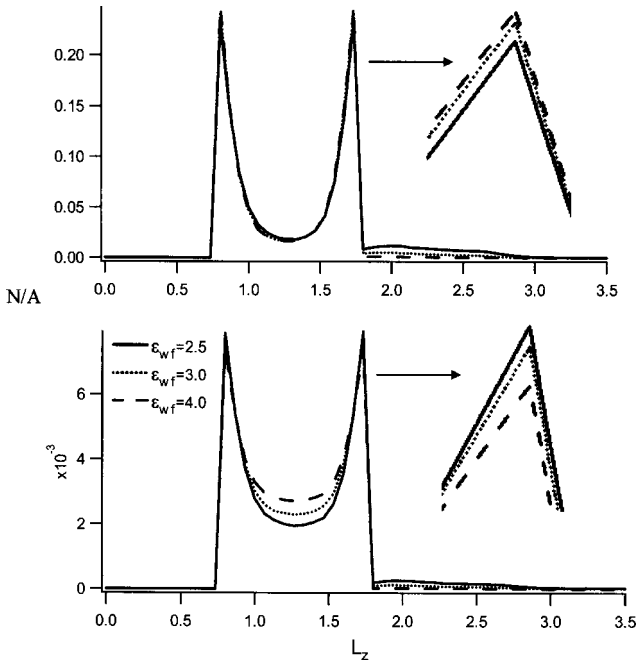

FIG. 6. Plot of density profile of thin-thick film for varied wall-fluid interaction strengths at temperature $T^*=0.68$. Upper region presents the density profile of thick film, whereas the lower region displays the density profile of thin film.

stronger wall-fluid affinity; consequently beyond the wall-fluid interaction range, $L_z=1.8$, the molecules for the lower wall-fluid affinity system tend to stick together, leading to higher density compared to higher wall-fluid affinity system. It is the density at position larger than $\lambda_{wf}=1.8$ from the wall appears to make a considerable impact on the overall number density of the thin and thick films. As wall-fluid interaction increases, the thick-film density decreases.

The effect of wall-fluid affinity is much stronger at higher temperature, consequently, change in the surface critical behavior is observed with the change of wall-fluid interaction strength (see Fig. 5). Phase coexistence data of Table I are fitted to Eqs. (13) and (14) to obtain the critical points. The values of critical parameters for various wall-fluid interactions, shown by filled symbols in Fig. 5, are listed in Table II. Finite size effect is found to be prominent for temperatures greater than $T^*=0.74$, hence to remove the system size effect, the number of particles were increased to 500, which led to increase the simulation box size to $20\times20\times20$. Critical exponent calculated in this work via least squares fit of the coexistence data using Eq. (13) is far from two-dimensional Ising value, 1/8. It is argued that finite size scaling[38,39] is necessary for such calculation as shown by Müller and MacDowell for thin-thick film,[36] however, a thorough analysis of critical properties of the current system via finite size scaling is reserved for a future study.

One of the objectives of this work was to use MD to obtain phase densities, pressure tensor components, and boundary tension. Figure 7 presents the pressure components profile along the x direction for wall-fluid interaction $\varepsilon_{wf}=3.0$ at $T^*=0.62$ and 0.68. Pressure components P_{xx} and P_{yy} are observed to agree with each other within the thin- and thick-film phases. Noise level in the simulated data is more

TABLE I. Thin-thick film coexistence data obtained from GC-TMMC simulations of SW fluid with varied wall-fluid affinity, $\varepsilon_{wf}=2.5$, 3.0, and 4.0. Surface coexistence densities for thick $(N/A)_l$ and thin $(N/A)_v$ films are calculated for a system size $L_x\times L_y=81$. For higher temperatures ($T^*\geqslant0.74$), a system size of $L_x\times L_y=400$ was used for coexistence density calculations. The errors are not indicated, where the error is an order of magnitude smaller than the last significant digit.

	T^*	$(N/A)_v$	$(N/A)_l$	P^*
$\varepsilon_{wf}=2.5$				
	0.62	0.028 03(1)	1.3818(1)	0.00 76
	0.65	0.042 91(6)	1.3522(9)	0.001 16
	0.68	0.064 73(4)	1.3149(7)	0.001 72
	0.7	0.085 23(3)	1.2802(12)	0.002 205
	0.72	0.113 1(1)	1.2414(7)	0.002 785
	0.74	0.154 0(120)	1.1854(16)	0.003 495
	0.75	0.180 4(36)	1.1533(39)	0.003 895
	0.76	0.223 4(35)	1.1010(14)	0.004 350(10)
	0.77	0.259 1(23)	1.0618(24)	0.004 840(10)
	0.78	0.323 8(28)	0.9925(1)	0.005 375
$\varepsilon_{wf}=3.0$				
	0.62	0.026 48(13)	1.3318(23)	0.000 695
	0.65	0.040 93(10)	1.2906(01)	0.001 065
	0.68	0.063 04(08)	1.2396(10)	0.001 58
	0.7	0.085 32(01)	1.1933(10)	0.002 025
	0.72	0.118 05(41)	1.1367(11)	0.002 57
	0.74	0.178 44(130)	1.0527(19)	0.003 25
	0.75	0.220 89(94)	0.9967(27)	0.003 645(1)
	0.76	0.283 08(1617)	0.9138(194)	0.004 085
$\varepsilon_{wf}=4.0$				
	0.62	0.025 40(7)	1.3162(14)	0.000 655
	0.65	0.039 35(4)	1.2628(13)	0.000 995
	0.68	0.061 71(13)	1.1991(10)	0.001 465
	0.7	0.085 23(21)	1.1445(28)	0.001 875
	0.72	0.123 00(144)	1.0753(20)	0.002 39
	0.74	0.205 35(920)	0.9540(122)	0.003 035
	0.75	0.270 14(2912)	0.8863(104)	0.003 420(10)

for the case of thick-film as expected due to higher surface density. Near the thin-thick interface we observe a sharp change in the sign of P_{yy}. The difference in the two components near the interface contributes to the boundary tension [see Eq. (10)]. Consequently, increase in the difference of pressure components increases the boundary tension. In Fig. 7, we can observe that the difference is greater at lower temperature. We further analyzed the contribution to the boundary tension as a function of the distance perpendicular to the substrate (i.e., along the z direction). We observed that the behavior (figure not shown) is similar to the nature of density profiles (see Fig. 6). Contribution to the boundary tension is significant only by the first two layers of the inho-

TABLE II. Prewetting critical temperature T_{cpw}^*, critical surface density $(N/A)_c$, and critical exponent β_c for SW fluid with respect to wall-fluid affinity ε_{wf}. Critical parameters are calculated using Eqs. (13) and (14).

ε_{wf}	T_{cpw}^*	$(N/A)_c$	β_c
2.5	0.7868(6)	0.6556(4)	0.2287(62)
3.0	0.7658(29)	0.5998(6)	0.2324(155)
4.0	0.7558(16)	0.5722(39)	0.2412(13)

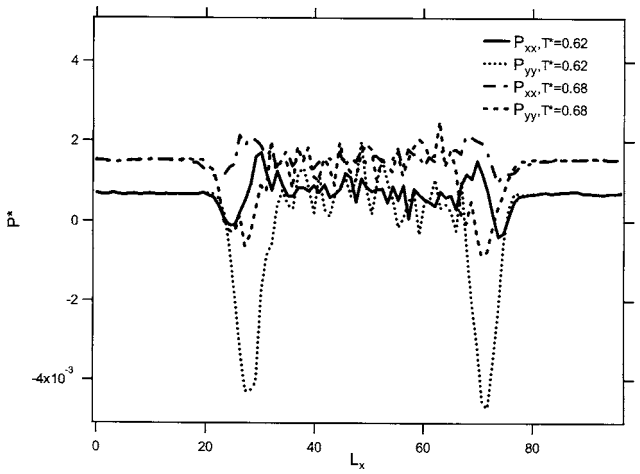

FIG. 7. Pressure profiles $P_{xx}(x)$ and $P_{yy}(x)$ of SW fluid for wall-fluid interaction strength, $\varepsilon_{wf}=3.0$ at $T^*=0.62$ and 0.68.

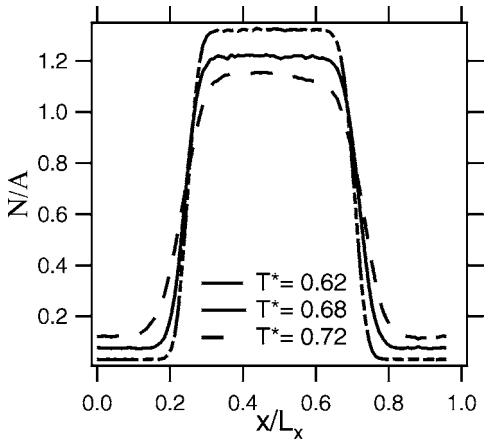

FIG. 9. Thin-thick film density profile obtained from MD simulation of SW fluid for wall-fluid affinity, $\varepsilon_{wf}=3.0$, with varied temperatures $T^*=0.62$, 0.68, and 0.72.

mogeneous film. Increase in the temperature ($T^* < T^*_{\mathrm{cpw}}$) does reduce the contribution from each layer of the film; however, the behavior is still akin to the density profile at higher temperature. Figure 8 presents the pressure component perpendicular ($P^*_{xx}=P^*=P\sigma^3/\varepsilon_{ff}$) to the thin-thick film interface (i.e., saturation pressure via MD) and compares with that from GC-TMMC. The data are being plotted in a Clausius-Clayperon form. The results from MD and GC-TMMC are in excellent agreement. Equilibrium pressure decreases as the wall affinity increases. Slope of the curve, however, is not sensitive to the wall-fluid affinity.

Figure 9 presents the surface density profile (N/A) versus inhomogeneous axis (i.e., L_x) for the two coexistence phases. Isotherms are being plotted for a constant wall-fluid interaction. Akin to vapor-liquid transition, we observe a similar behavior in the density profile of thin-thick film transition. Sharpness of the interface decreases with the increase in the temperature, which indicates the increase in the interfacial width. Similar to vapor-liquid interfacial tension, one can connect the interfacial width with the boundary tension; boundary tension should go to zero as the interfacial width approaches to infinity (at prewetting critical temperature). Figure 10 presents the surface density profile for various wall-fluid affinities at a constant temperature. Effect on the interfacial width is not as drastic as we observed in Fig. 9. Nevertheless, we can see that thick-film density decreases with increase of the wall-fluid affinity, as also seen from Fig. 5 of the surface phase coexistence. Because of the change in the thick-film density, interfacial width appears to decrease (calculation is not shown) with the increase in the wall-fluid affinity.

We took two approaches to investigate the influence of wall-fluid affinity on the behavior of boundary tension. Binder's formalism is employed to calculate the boundary tension of the infinite system size from a set of finite system size calculations. Since the wall-fluid affinity, $\varepsilon_{wf}=3$, exhibits the prewetting phenomenon, the value of $\varepsilon_{wf}=3$ is selected to explore size effects of the system. Figure 11 presents the finite size scaling plot of boundary tension values for temperatures $T^*=0.68$ and 0.72. Scaling behavior is found to be linear as also observed by Errington for model argon on solid carbon dioxide system.[19]

Figure 12 presents the boundary tension ($\tau^*=\tau\sigma_{ff}/\varepsilon_{ff}$)

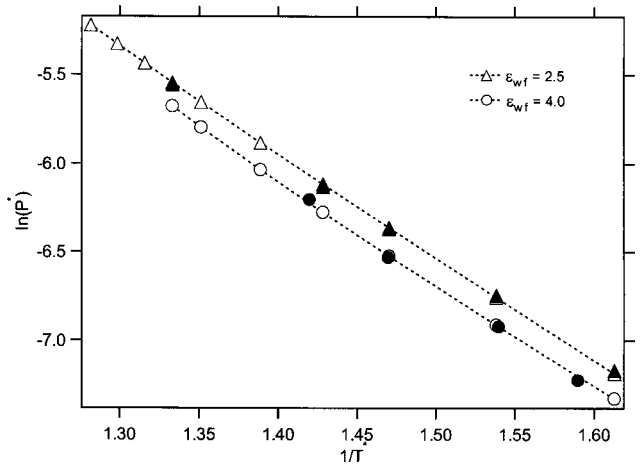

FIG. 8. Saturation pressure curve for thin-thick film of SW fluid for two values of wall-fluid affinity, $\varepsilon_{wf}=2.5$ and 4.0. Equilibrium pressure values from MD simulation are shown as filled symbols and those from GC-TMMC are shown as open symbols with dotted lines, which are guides to an eye.

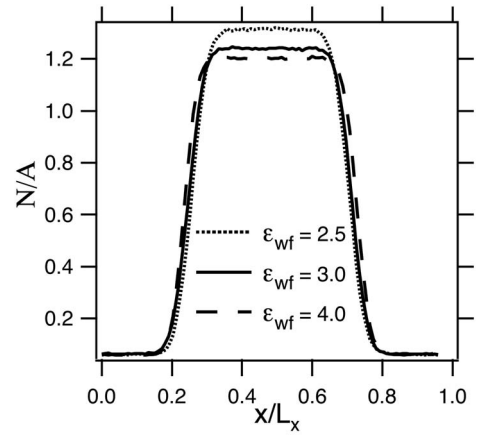

FIG. 10. Thin-thick film density profile obtained from MD simulation of SW fluid for temperature $T^*=0.68$ with varied wall-fluid affinity, $\varepsilon_{wf}=2.5$, 3.0, and 4.0.

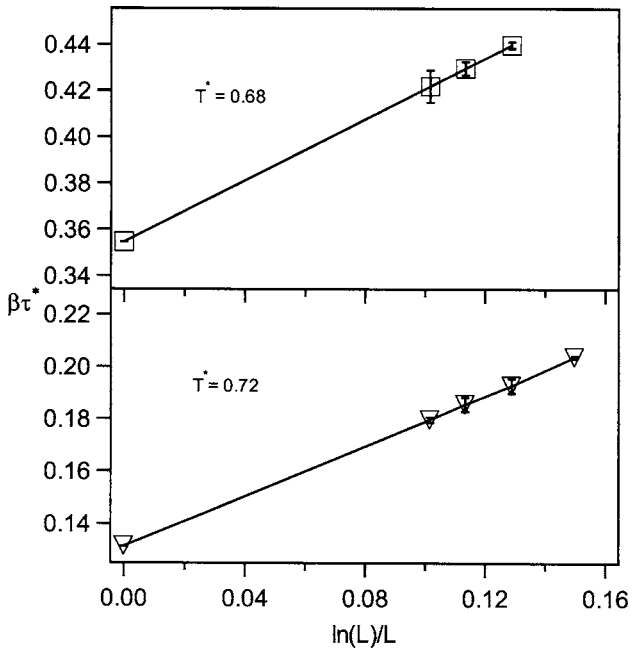

FIG. 11. Finite size boundary tension as a function of the system size for temperatures $T^*=0.68$ (upper plot) and 0.72 (lower plot). Open symbols represent the simulation data and the solid line shows an extrapolation of boundary tension at infinite system size. Simulation data are collected for system sizes with $20 \leqslant L \leqslant 40$.

of thin-thick films for two different wall-fluid strengths. The data summarized in Table III are generated using GC-TMMC+FSS and MD. The agreement between two methods is excellent. Boundary tension of thin-thick SW films decreases with increase of the temperature, similar to vapor-liquid bulk surface tension; however, at a constant temperature boundary tension increases with decrease in the wall-fluid affinity. The decreasing value of boundary tension can be attributed to lower free energy of the two-phase system with respect to the interface as the wall-fluid affinity increases at a constant temperature. We have observed that, for the current set of parameters, interfacial free energy does

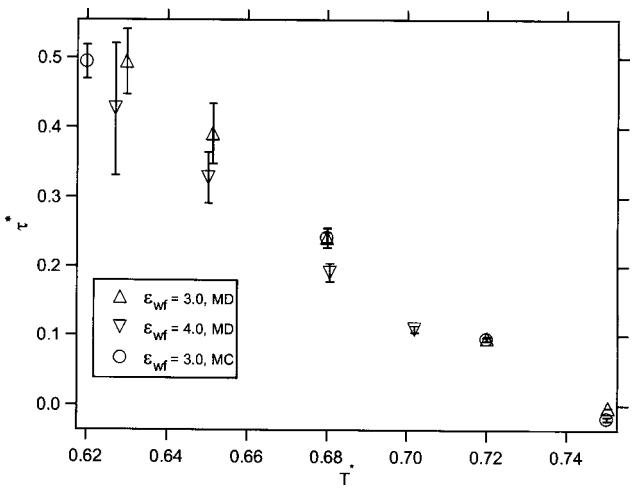

FIG. 12. Comparison of the thin-thick film boundary tension values from MD and GC-TMMC+FSS simulations as a function of temperature. Open circles are the line tension values from MC simulation for $\varepsilon_{wf}=3.0$. MD simulation data are represented by triangles.

TABLE III. MD simulation results of boundary tension for SW fluids over a homogeneous solid surface with wall-fluid affinities $\varepsilon_{wf}=3.0$ and 4.0.

$\varepsilon_{wf}=3.0$		$\varepsilon_{wf}=4.0$	
T^*	τ^*	T^*	τ^*
0.6299	0.494(46)	0.6271	0.426(94)
0.6617	0.381(15)	0.6503	0.328(36)
0.6829	0.281(9)	0.6807	0.191(13)
0.7007	0.220(4)	0.7023	0.125(5)

not scale with the system size as dramatically as for the bulk system, leading to the requirement of very precise calculation (extensive sampling) for the finite size scaling. Hence, in practice, for the current system, MD method is found to be more effective than GC-TMMC+FSS for calculating interfacial properties especially at lower temperature.

IV. CONCLUSION

We studied the first order wetting transition of a SW fluid system using GC-TMMC and MD methods. In this work we investigate the effects of wall-fluid interaction on the prewetting transition and boundary tension. Surface phase-coexistence calculation was done using GC-TMMC. Saturation pressure and boundary tension via both methods are in good agreement. Prewetting transition is being observed for ε_{wf} in the range of 2.5–4.0. We observe increase in the prewetting critical temperature and density with the decrease of the surface affinity. Layering behavior is observed at higher wall-fluid affinity. We further investigated the usefulness of two molecular simulation methods for calculating the boundary tension. We observed that MD route is computationally more suitable for the calculation of boundary tension, for the present system, especially at lower temperature. Boundary tension increases with the decrease in temperature. Increase in the surface wall affinity reduces the boundary tension.

ACKNOWLEDGMENTS

This work was supported by the Department of Science and Technology, Government of India (Grant No. SR/S3/CE10/2006). We acknowledge further computational support from Computer Center, Indian Institute of Technology Kanpur.

[1] L. D. Gelb, K. E. Gubbins, R. Radhakrishnan, and M. S. Bartkowiak, Rep. Prog. Phys. **62**, 1573 (1999).
[2] J. W. Cahn, J. Chem. Phys. **66**, 3667 (1977).
[3] C. Ebner and W. F. Saam, Phys. Rev. Lett. **38**, 1486 (1977).
[4] H. T. Davis, *Statistical Mechanics of Phases, Interfaces and Thin Films* (Wiley-VCH, New York, 1996).
[5] J. E. Rutledge and P. Taborek, Phys. Rev. Lett. **69**, 937 (1992).
[6] R. B. Hallock, J. Low Temp. Phys. **101**, 31 (1995).
[7] J. A. Phillips, D. Ross, P. Taborek, and J. E. Rutledge, Phys. Rev. B **58**, 3361 (1998).
[8] G. M. E. Cheng, H. C. Lee, M. H. W. Chan, M. W. Cole, C. Carraro, W. F. Saam, and F. Toigo, Phys. Rev. Lett. **70**, 1854 (1993).
[9] F. Kruchten and K. Knorr, Phys. Rev. Lett. **91**, 085502 (2003).
[10] J. E. Finn and P. A. Monson, Phys. Rev. A **39**, 6402 (1989).
[11] W. Shi, X. Zhao, and J. Johnson, Mol. Phys. **100**, 2139 (2002).
[12] M. B. Sweatman, Phys. Rev. E **65**, 011102 (2001).
[13] S. Sokolowski and J. Fischer, Phys. Rev. A **41**, 6866 (1990).

[14] M. J. P. Nijmeijer, C. Bruin, and A. F. Bakker, Mol. Phys. **72**, 927 (1991).
[15] M. Fitzgerald, R. R. Picard, and R. N. Silver, Europhys. Lett. **46**, 282 (1999).
[16] B. A. Berg and T. Neuhaus, Phys. Rev. Lett. **61**, 9 (1992).
[17] A. M. Ferrenberg and R. H. Swendsen, Phys. Rev. Lett. **61**, 2635 (1988).
[18] J. R. Errington, Langmuir **20**, 3798 (2004).
[19] J. R. Errington and D. W. Wilbert, Phys. Rev. Lett. **95**, 226107 (2005).
[20] H. Liu, S. Garde, and S. Kumar, J. Chem. Phys. **123**, 174505 (2005).
[21] F. del Rio, E. Avalos, R. Espindola, L. F. Rull, G. Jackson, and S. Lago, Mol. Phys. **100**, 2531 (2002).
[22] J. R. Elliot and L. Hu, J. Chem. Phys. **110**, 3043 (1999).
[23] G. Orkoulas and A. Z. Panagiotopoulos, J. Chem. Phys. **110**, 1581 (1999).
[24] J. K. Singh, D. A. Kofke, and J. R. Errington, J. Chem. Phys. **119**, 3405 (2003).
[25] L. Vega, E. de Miguel, L. F. Rull, G. Jackson, and I. A. McLure, J. Chem. Phys. **96**, 2296 (1992).
[26] P. Orea, Y. Duda, and J. Alejandre, J. Chem. Phys. **118**, 5635 (2003).
[27] J. K. Singh and S. K. Kwak, J. Chem. Phys. **126**, 024702 (2007).
[28] J. R. Henderson and F. V. Swol, Mol. Phys. **56**, 1313 (1985).
[29] P. Bolhuis, M. Hagen, and D. Frenkel, Phys. Rev. E **50**, 4880 (1994).
[30] N. Asherie, A. Lomakin, and G. B. Benedek, Phys. Rev. Lett. **77**, 4832 (1996).
[31] E. Zaccarelli, G. Foffi, K. A. Dawson, F. Sciortino, and P. Tartaglia, Phys. Rev. E **63**, 031501 (2001).
[32] A. Lomakin, N. Asherie, and G. B. Benedek, J. Chem. Phys. **104**, 1646 (1996).
[33] Y. Zhou, M. Karplus, J. M. Wichert, and C. K. Hall, J. Chem. Phys. **107**, 10691 (1997).
[34] K. Binder, Phys. Rev. A **25**, 1699 (1982).
[35] M. P. Allen and D. J. Tildesley, *Computer Simulation of Liquids* (Clarendon, Oxford, 1987).
[36] M. Muller and L. G. MacDowell, Macromolecules **33**, 3902 (2000).
[37] D. A. Kofke and B. C. Mihalick, Fluid Phase Equilib. **194–197**, 327 (2002).
[38] A. D. Bruce and N. B. Wilding, Phys. Rev. Lett. **68**, 193 (1992).
[39] N. B. Wilding, J. Phys.: Condens. Matter **9**, 585 (1997).